Analyst

PAPER

View Article Online
View Journal

Cite this: DOI: 10.1039/d5an01220a

Electrokinetic separation of bacteriophage ϕKZ from bacterial cells

Viswateja Kasarabada, [a] Zakia Azad,[b] Julie A. Thomas*[b] and Blanca H. Lapizco-Encinas *[a]

Received 19th November 2025,
Accepted 6th March 2026

DOI: 10.1039/d5an01220a

rsc.li/analyst

The rise of drug-resistant bacteria and nosocomial infections has intensified the need for alternative antimicrobial strategies such as phage therapy. However, clinical adoption remains hindered by the lack of easily adoptable, high-yield purification methods. This study presents the first report of the electrophoretic separation of bacteriophage ϕKZ from binary mixtures with microparticles and *Escherichia coli* cells. Insulator-based electrokinetic (iEK) microchannels were employed to exploit the differences in electrophoretic migration and the nonspecific binding affinity of bacteriophages to the surfaces of both microparticles and bacterial cells. The electrophoretic mobilities of all analytes were characterized in isolation in a uniform rectangular microchannel. Additionally, the microparticles and *E. coli* cells were also characterized in the presence of ϕKZ to assess the effect of nonspecific binding, which resulted in the reduction in zeta potential of up to approximately 8 mV. Subsequently, employing the mobility data, COMSOL Multiphysics was utilized to identify the appropriate separation voltages to be used in the iEK channels. Separations under the streaming electrokinetic regime were carried out at the field strengths of 194.3 V cm^{-1} and 430.4 V cm^{-1}. Furthermore, an additional trapping–streaming separation experiment between *E. coli* cells and ϕKZ was achieved at 580.6 V cm^{-1}. These findings demonstrate the feasibility of a novel electrokinetic-based purification strategy for the rapid and scalable isolation of bacteriophages.

Introduction

The crisis of drug-resistant bacteria is escalating. According to 2019 data from the U.S. Centers for Disease Control (CDC), these infections were responsible for an estimated 687 000 cases and 72 000 deaths, costing the U.S. healthcare system over $25 billion.[1,2] This escalation poses an immediate threat to human life and a major burden on the global economy. A promising treatment option is the use of bacteriophages (phages), which are viruses that selectively target specific bacteria.[3] Phages represent the most abundant biological entities in the procaryotic order of the biosphere.[4] The earliest documentation of phages involved the independent discoveries by the English bacteriologist Frederick Twort in 1915, while working with the cultures of smallpox vaccine, and by the French physician Félix d'Hérelle in 1919, while attempting to treat dysentery.[5,6] The key advantage of using phages to treat bacterial infections is their host specificity, limiting their ability to infect non-target species despite their diverse evolution.[5] Additionally, phages are abundant in the environment and are genetically diverse.[7,8] For instance, the phage ϕKZ utilized in this study is highly host-specific, replicating exclusively within the bacterium *Pseudomonas aeruginosa*.[9] Because of this specificity, ϕKZ and related phages have been historically used to treat *P. aeruginosa* infections.[10,11] However, in the current era, phage therapy faces significant challenges before reaching its full clinical potential.[12–14] A primary concern is the presence of endotoxins and enterotoxins from lysed host cells can induce adverse effects in patients undergoing therapy.[15] Developing a reliable and easily adoptable purification method is essential to mitigate this risk. Current purification methodologies include polyethylene glycol (PEG) precipitation, cesium chloride (CsCl) aided ultracentrifugation, ultrafiltration and column chromatography, among others.[16–21]

An ideal phage purification strategy for clinical applications must address four critical parameters: phage recovery rate, endotoxin removal efficiency, scalability and speed. Most prevalent methods excel in only one or two of these areas and fail to meet all four criteria simultaneously.[22–28] For instance, high-purity methods such as the purification protocol published by Luong *et al.* require a 3.5-day window for purifying an isolated phage sample from the initial phage plaque isolation.[21] Furthermore, the ultrafiltration and ultracentrifugation steps involved in these methods are time-consuming and

[a]*Microscale Bioseparations Laboratory and Biomedical Engineering Department, Rochester Institute of Technology, 160 Lomb Memorial Drive, Rochester, New York, 14623, USA. E-mail: bhlbme@rit.edu*
[b]*Thomas H. Gosnell School of Life Sciences, Rochester Institute of Technology, Rochester, NY 14623, USA. E-mail: jatsbi@rit.edu*

rely on specialized equipment that lacks global ubiquity in clinical laboratories. A promising solution lies in microfluidic devices utilizing electrokinetics (EK), which offer portability, speed and a label-free approach capable of purifying phage samples in a matter of minutes.[29–34]

Electrophoresis (EP), defined as the movement of charged particles suspended in a liquid medium under the influence of an electric field, is a cornerstone separation technique in analytical chemistry. Electrophoresis can be further subdivided into linear electrophoresis (EP_L) and nonlinear electrophoresis (EP_{NL}). Arne Tiselius first reported on EP_L in 1937.[35] Since then, several modes of EP_L have been developed, including capillary zone electrophoresis (CZE), for the manipulation of intact microorganisms.[36]

In general, EP_L is an effective separation technique that exploits differences in electrical charge between target analytes. In contrast, EP_{NL} is a more complex phenomenon that is influenced by particle size and shape.[37,38] Recently, EP_{NL} has received significant attention as a powerful separation technique.[39,40] Although EP_{NL} was first reported by Dukhin and associates in the early 1970s,[40–44] the field has only recently begun to make significant progress.[45–47]

The first reported use of EK phenomena for virus purification was by J. B. Bancroft in 1962, who employed EP to purify bean pod mottle virus.[48] Kremser *et al.* reviewed the use of CZE in manipulating viruses, bacteria and eukaryotic cells.[49,50] Serwer and Hayes reported in 1982 the use of agarose gel EP for the fractionation of T7 bacteriophages.[51] They observed a concentration effect where bands of T7 phage formed, possibly due to the adherence of positively charged tail fibers to the agarose gel. For further information, the reader is referred to two recent reviews on the recent advancements in the use of EK methods in microfluidic devices for the manipulation and rapid assessment of microorganisms.[33,36]

Dielectrophoresis (DEP), a phenomenon that depends on the polarizability of a particle with respect to that of the suspending medium, is another EK phenomenon used to manipulate microorganisms in microscale systems. Numerous studies have reported the use of DEP to manipulate, trap, or separate a wide range of microbes.[52] The Green research group employed DEP to characterize the dielectric properties of Herpes Simplex Virus type 1 and manipulate these viruses within microelectrode array devices.[53–56] More recently, the Hayes research group has extensively utilized insulator-based dielectrophoresis (iDEP) within rectangular channels featuring sawtooth constrictions to distort the electric field, enabling the purification and isolation of various viruses.[57–59] In 2019, Coll de Peña *et al.*[60] investigated the application of insulator-based EK (iEK) systems to purify bacteriophages SPN3US, ϕKZ and 201ϕ2-1, while assessing their post-process viability.

The present study also employed an iEK system, which is depicted in Fig. 1. This type of device contains insulating structures within the channel that create regions with higher field intensities where nonlinear EK phenomena, such as DEP and EP_{NL}, are enhanced. Recent findings in iEK systems stimulated with DC or low-frequency AC electric fields suggest that DEP may not be a dominant EK phenomenon, suggesting instead that EP effects (both EP_L and EP_{NL}) are the dominant mechanisms governing particle electromigration.[46,61]

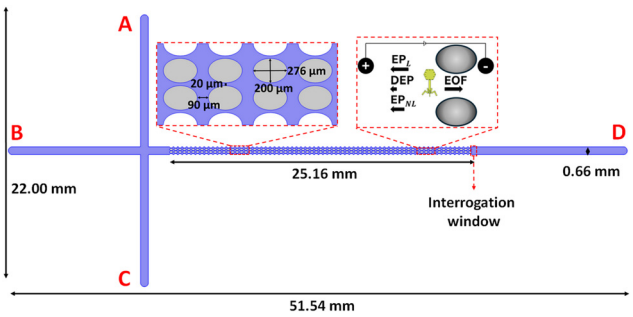

Fig. 1 Illustration of the iEK channel employed for this study, depicting the channel dimensions. The left inset shows the post shapes and their dimensions, while the right inset illustrates the forces a particle inside this channel would experience before entering the constriction space between two posts. The window at the end of the post array indicated by a red box is the interrogation window where fluorescence measurements are taken.

Lomeli-Martin *et al.*[62] recently analyzed bacteriophages SPN3US and ϕKZ and determined their electrophoretic mobilities and zeta potential. The findings of Coll de Peña[60] and Lomeli-Martin form the basis for this work.

This study investigates the binary separation of bacteriophage ϕKZ from two analytes: (1) polystyrene microparticles (P1), and (2) live *Escherichia coli* cells. These bacterial cells were used as proxies for the host cell, *P. aeruginosa*. Since *P. aeruginosa* is an airborne pathogen that poses a risk of aerosol transmission,[63] a safer bacterial proxy was selected for this study. Previous reports indicate that *P. aeruginosa* has a zeta potential range of −25 to −35 mV[64,65] and a mean hydrodynamic diameter D_h of 0.7 to 2.0 μm.[66] Therefore, the *E. coli* strain used in this study with a mean zeta potential of −25.5 mV and a D_h of 1.8 μm serves as an ideal proxy. Similarly, 1.0 μm microparticles were chosen as the synthetic proxy for this experiment due to their nearly identical zeta potential (−25.5 mV) to the *E. coli* strain. The electrophoretic mobilities of phage ϕKZ, microparticles and *E. coli* cells were characterized in a uniform rectangular microchannel under linear and nonlinear regimes by employing an established protocol.[62] Although bacteriophages are known to exhibit nonspecific binding to non-host bacteria and synthetic surfaces,[67–69] the electrokinetic consequences of these interactions remain uncharacterized.

Typically, this nonspecific binding is driven by a combination of electrostatic interactions, van der Waals forces, and hydrophobic effects, where the amphoteric nature of the phage capsid allows it to adsorb to diverse surfaces depending on the local environment.[70] To date, few studies have quantified how this binding alters the fundamental surface properties of host or non-host surfaces. However, it is known that

the positively charged tail fibers of T4 phages target negatively charged bacterial surface receptors.[71]

Bacteriophage ϕKZ is a myovirus meaning its virion is composed of a proteinaceous icosahedral capsid, which contains the dsDNA genome, and a contractile tail that ends in a baseplate structure used to recognize and bind to the host cell. Previous studies have shown that the ϕKZ virion is unusually large and complex for a tailed phage and that it possesses unusual features, including many long fibers that emanate from its contractile tail, in addition to the fibers on its baseplate.[72–74] Since the major virion proteins that form the ϕKZ virion share divergent homologs to those of the model *E. coli* phage T4, it is likely that the ϕKZ tail is positively charged, similar to that of T4.[75,76] Due to these characteristics of the ϕKZ virion, it was hypothesized that bacteriophage ϕKZ adheres to the surfaces of the microparticles P1 and *E. coli* cells used in this study. Characterization studies were conducted for the microparticles and *E. coli* cells to quantify this effect in terms of changes in zeta potential. These characterization data were then input into a COMSOL Multiphysics model to identify the appropriate voltages required for successful binary separation of phages from microparticles and *E. coli* cells within T-shaped iEK channels containing oval-shaped posts (Fig. 1). The results of this study demonstrate successful binary separations, in the streaming and streaming–trapping electrokinetic modes, by combining linear and nonlinear electrophoretic effects. This study also aims to understand the changes in the zeta potential of microparticles and *E. coli* cells as a result of nonspecific binding.

Theory

Electrokinetic phenomena are classified as linear or nonlinear, contingent on their relationship with the electric field magnitude. Three dimensionless parameters are employed to classify EK phenomena. These parameters are: the dimensionless field strength (β), the Peclet (Pe) and Dukhin (Du) numbers, defined as follows:

$$\beta = \frac{E\alpha}{\varphi_T} \tag{1}$$

$$\mathrm{Du} = \frac{K^{\sigma}}{K_m \alpha} \tag{2}$$

$$\mathrm{Pe} = \frac{\alpha|(v_{EP})|}{D} \tag{3}$$

where φ_T is the thermal voltage, α is the particle radius, K^{σ} is the surface conductivity, K_m is the bulk conductivity of the suspending medium, v_{EP} is the electrophoretic velocity of the particle, and D is the diffusion coefficient. The values of the dimensionless parameters used in the characterization of the target particles in this study are reported in Table S1 of the SI.

The linear EK phenomena present in the microchannels used in this study are EO and EP_L. The velocity expressions for EO flow and EP_L following the Helmholtz–Smoluchowski (HS) approximation are:[77]

$$v_{EO} = \mu_{EO}E = -\frac{\varepsilon_m \zeta_W}{\eta}E \tag{4}$$

$$v_{EP,L} = \mu_{EP,L}E = \frac{\varepsilon_m \zeta_P}{\eta}E \tag{5}$$

for $\kappa\alpha \gg 1$, $\beta \ll 1$, Du ~ 0, and Pe $\ll 1$ (weak field regime); where v and μ represent the velocity and mobility, respectively; E is the electric field, κ is the inverse of the Debye length ($\kappa = \lambda_D^{-1}$); ζ_W and ζ_P are zeta potentials of the wall and particle, respectively; ε_m and η denote the permittivity and viscosity of the suspending medium, respectively.

The HS approximation for EP_L is only valid for particles with sizes significantly larger than the Debye length of the EDL, *i.e.*, $\kappa\alpha \gg 1$. This is not the case for the phage ϕKZ considered in this study. While the Debye length of the EDL in the suspending medium used in this work was estimated to be ≈14 nm, the hydrodynamic radius ($\alpha = D_h/2$) of the phage is 78 nm, making the HS approximation ($\kappa\alpha = 5.6$) inapplicable. For $\kappa\alpha \geq 1$, *i.e.*, smaller particles, Henry's formula was considered appropriate and employed for this study:[78]

$$v_{EP,L} = \mu_{EP,L}E = \frac{2\varepsilon_m \zeta_P}{3\eta} f(\kappa\alpha)E \tag{6}$$

for $\kappa\alpha \geq 1$, $\beta \ll 1$, Du ~ 0, and Pe $\ll 1$

$$f(\kappa\alpha) = \left[1 + \frac{1}{2\left(1 + \frac{2.5}{\kappa\alpha(1+2e^{-\kappa\alpha})}\right)^3}\right] \tag{7}$$

The nonlinear EK phenomena considered in this study are EP_{NL} and DEP. There are several models that describe EP_{NL} by utilizing the parameters β, Pe, and Du. Expressions for $v_{EP,NL}$ have been developed for the two limiting cases of small Pe (Pe $\ll 1$) and high Pe (Pe $\gg 1$) known as moderate and strong field regimes, respectively. The expressions of $v_{EP,NL}$ for the two limiting cases are given below:[79–81]

$$v_{EP,NL}^{(3)} = \mu_{EP,NL}^{(3)} E^3 \hat{a}_E \tag{8}$$

for $\beta \leq 1$, Pe $\ll 1$ (moderate field regime)

$$v_{EP,NL}^{(3/2)} = \mu_{EP,NL}^{(3/2)} E^{3/2} \hat{a}_E \tag{9}$$

for $\beta > 1$, Pe $\gg 1$ (strong field regime); where $E = E \cdot \hat{a}_E$, E is the electric field magnitude and $\hat{a}_E$ is the unit vector of the applied electric field; $\mu_{EP,NL}^{(n)}$ denotes EP_{NL} mobility, and n denotes the dependence of $v_{EP,NL}^{(n)}$ with E (Table S2). Recently, the Xuan research group investigated the dependence of EP_{NL} on particle size and shape; yet, a unified analytical expression for nonspherical particles is not yet available.[82,83] Consequently, a spherical particle model employing D_h—computed from the shape and size of the bacteria and bacteriophages—was adopted for this study. Given the magnitude of electrical fields used in this work, only the moderate field regime ($i = 3$) of EP_{NL} is considered in this study.

The expression for v_{DEP} of a spherical particle is:

$$v_{DEP} = \mu_{DEP}\nabla E^2 = \frac{\alpha^2 \varepsilon_m}{3\eta}\mathrm{Re}[f_{CM}]\nabla E^2 \quad (10)$$

where $\mathrm{Re}[f_{CM}]$ is the real part of the Clausius–Mossotti factor, which accounts for the relative polarization of the particles to that of the suspending medium, and ∇E^2 is the gradient of the square of electric field magnitude E. While small compared to the bulk electrophoretic velocity, the DEP vector contributes to the overall migration behavior of the particle. Including this term allows the COMSOL model to be applicable across a wider range of voltages. Furthermore, incorporating DEP effects improves the overall particle velocity estimation for accuracy purposes.[61] Thus, the overall velocity of the particles inside the iEK system considered in this study is determined by following the expression,

$$v_P = v_{EO} + v_{EP,L} + v^{(3)}_{EP,NL} + v_{DEP} \quad (11)$$

The quality of the separations conducted in this study was determined from the separation resolution R_s obtained by analyzing the electropherogram of the particles measured in the interrogation window (see Fig. 1). It is expressed as follows:

$$R_s = \frac{2(t_{R2,e} - t_{R1,e})}{W_1 + W_2} \quad (12)$$

where W is the width of the peak at its base and $t_{R,e}$ is the experimental retention time of each particle peak in the post array of the iEK channel.

Materials and methods

Suspending medium and particles

The suspending medium was a 0.2 mM solution of K_2HPO_4 with 0.05% (v/v) Tween-20 added to prevent clumping. The conductivity and pH of the medium were measured to be 42.5 ± 2.8 μS cm^{-1} and 7.2 ± 0.1, respectively; resulting in a μ_{EO} and ζ_W of $(4.7 \pm 0.3) \times 10^{-8}$ m^2 V^{-1} s^{-1} and −60.1 ± 3.7 mV, respectively, characterized through current monitoring experiments.[84] The study employed a total of three target particles – a 1.0 μm polystyrene particle, *E. coli* bacteria, and phage ϕKZ. Bacteriophage ϕKZ was prepared in a *P. aeruginosa* bacterial culture and to eliminate as much bacterial debris as possible, the phage stock was centrifuged twice at 7700 *g* for 10 min at 4 °C resulting in a titer of 2×10^{11} PFU mL^{-1} (PFU – plaque forming units). This study also employed *E. coli* cells (ATCC: 11775, American Type Culture Collection, Manassas, VA). Standard cell culture protocols were followed to obtain an *E. coli* sample. Standard labeling protocols were used to label ϕKZ phages and *E. coli* cells with SYBR Gold and SYTO 85 dyes (Invitrogen, Carlsbad, CA) staining them green and red, respectively. Fluorescent polystyrene particles (Red, Magsphere, Pasadena, CA) with a diameter of 1 μm were suspended in the medium and employed as a synthetic proxy for *P. aeruginosa* cells. The particle concentrations employed in this study are provided in Table S3 of the SI. All particles were characterized in a post-less rectangular microchannel to obtain the parameters of ζ_P and $\mu^{(3)}_{EP,NL}$ using particle tracking velocimetry (PTV) experiments (Table 1).[46,62,85,86] Given that bacteriophage ϕKZ and *E. coli* cells are non-spherical, their equivalent D_h values were utilized for zeta potential determination using Henry's function and the Smoluchowski approximation, respectively. Bacteriophages are known to bind non-specifically to non-host cells as well as synthetic surfaces.[67,68] To quantify this interaction, *E. coli* cells and P1 microparticles were characterized in the presence of the ϕKZ phages. The changes observed in the EK properties of the *E. coli* cells and microparticles P1 due to the presence of the phage ϕKZ are discussed in the Results section. The suspending medium influences particle characteristics, making these properties specific to this particle–liquid system. The particles were mixed at the desired concentrations (Table S3) and were injected into the iEK device using a three-step EK injection process.[87]

Microdevices

The characterization studies were conducted in a uniform rectangular postless microchannel that was 40 μm deep, 1.1 mm wide, and 1 cm long. Separation studies were conducted in T-shaped iEK microchannels containing insulating posts, featuring a depth of 40 μm. The schematic and dimensions of the iEK channel are shown in Fig. 1. All devices were made from polydimethylsiloxane (PDMS, Dow Corning, MI, USA) using standard soft lithography techniques.[88] After PDMS curing and the punching of holes in the microchannels for the four reservoirs (see Fig. 1 reservoirs A, B, C, D), the PDMS devices were attached to a PDMS-coated glass wafer through corona treatment followed by heat treatment. The microchannels were filled with the suspending medium at least 12 hours before experimentation to ensure a well-developed EDL and, thereby, a stable EO flow.

Equipment and software

Electric potentials were applied through platinum wire electrodes using a high-voltage power supply (model HVS6000D, LabSmith, Livermore, CA). Experiments were recorded with a Leica DMi8 inverted microscope (Wetzlar, Germany). Tracker software (Douglas Brown), built on the Open-Source Physics (OSP)[89] Java framework, was used to analyze PTV experiment

Table 1 Characteristics of the particles used in this study. The conditions under which the zeta potential and the mobility of EPNL were determined are listed in the SI in Tables S1 and S2

Particle ID	Species present	D_h (nm)	ζ_P (mV)	$\mu^{(3)}_{EP,NL} \times 10^{-19}$ (m^4 V^{-3} s^{-1})
ϕKZ	Solo	156	−50.3 ± 3.1	−3.1 ± 0.3
Microparticle (P1)	Solo	1000	−25.5 ± 0.9	−15.3 ± 3.5
	With ϕKZ		−20.2 ± 0.3	−24.4 ± 1.7
E. coli cells	Solo	1800	−25.5 ± 1.5	−64.2 ± 9.4
	With ϕKZ		−17.6 ± 0.6	−63.3 ± 5.4

data, while ImageJ was used to analyze the integrated pixel density of the videos recorded for separation experiments.

Mathematical model

Mathematical modeling is a valuable tool to guide EK experimentation and device design.[90] Numerical models were constructed in COMSOL Multiphysics for the device used in this study (Fig. 1) using the experimentally determined characteristics (Table 1) as inputs to predict the electric field (Fig. S3) and the particle retention times ($t_{R,p}$) which were compared with the experimental retention times ($t_{R,e}$). Detailed information about the COMSOL model and the conditions employed to obtain the predicted retention times are included in Fig. S1, S2 and Tables S4, S5 of the ESI. The COMSOL model used in this study is used to identify operational voltages for the injection window of the experiment (Table 2). It does not account for the electric field distortions created by the target particles themselves, particle–particle interactions, temperature changes such as Joule heating, or injection bias during the EK injection process. The cutline shown in Fig. S2 was used to obtain $t_{R,p}$ *vs.* applied electric potential data. Applied electric potentials that would lead to a difference in predicted retention times ($\Delta t_{R,p}$) of more than 90 s were used as a starting point. A summary of the input voltages *versus* the differences in retention time ($\Delta t_{R,p}$) for both the streaming separation experiments is included in Table S6 of the SI, respectively.

Experimental procedure

Samples of mixed particle suspensions of 5 μL (concentrations in Table S3) were injected into reservoir A of the iEK device using a pipette, and platinum electrodes were placed into each of the reservoirs. To eliminate hydrodynamic bias, the pressure-driven flow was eliminated by carefully balancing the liquid levels in the four reservoirs. An EK injection process comprising the sequential application of three sets of voltages (*i.e.*, loading, gating, and injection, see Table 2)[87,91,92] was used to electrokinetically inject a small amount of the sample into the microchannel. The particles were recorded during their migration across the microchannel. The fluorescence signal used to build the electropherogram was obtained by focusing the camera focused on the interrogation window shown in Fig. 1.

Table 2 Voltage applied at the electrodes A–D for the EK injections for all separations. The injection steps for each separation have different durations and voltages at electrode B

		Applied voltage at each reservoir (V)			
Step	Duration (s)	A	B	C	D
Loading	12	800	200	0	500
Gating	4	800	800	700	−100
Injection for 194.3 V cm^{-1}	400	100	700	100	0
Injection for 430.4 V cm^{-1}	200	100	1800	100	0
Injection for 580.6 V cm^{-1}	100	100	2500	100	0

Results and discussion

Characterization of particles used in this study

In the Introduction, it was hypothesized that the large, potentially positively charged tail fibers of ϕKZ would induce nonspecific contact binding with negatively charged non-host surfaces, thereby altering their EK properties. To validate this hypothesis, characterization studies were conducted for the non-phage analytes used in this study in the presence of ϕKZ. It was found that P1 microparticles and *E. coli* cells exhibit different EK properties compared to when they are characterized individually in "solo" experiments. As detailed in Table 1, in both cases, a decrease in zeta potential magnitude was observed. The zeta potential of the microparticles changed from −25.5 mV to −20.2 mV when characterized solo *vs.* in the presence of ϕKZ, respectively. For *E. coli* cells, the zeta potential changed from −25.5 mV to −17.6 mV for solo *vs.* in the presence of ϕKZ, respectively. This reduction is attributed to the formation of nonspecific binding of bacteriophages on non-host surfaces, whether they are bacterial or synthetic. The process likely results from the natural affinity of positively charged tails encountering the negatively charged surfaces and thereby potentially creating ϕKZ-P1 or ϕKZ-*E. coli* complexes. While the native zeta potential difference between the phage ϕKZ and *E. coli* cells (~25 mV) was already sufficient for separation, this binding-induced reduction widened the gap to ~33 mV, providing a larger margin for discrimination. Regarding the mobility of EP_{NL} for all particles, the results are as expected, as the larger particles (P1 microparticles and *E. coli* cells) exhibited a much higher magnitude of their $\mu^{(3)}_{EP,NL}$ values than the small phages, which is agreement with previous reports.[85] An increase in particle size increases the convective-diffuse layer of the EDL, resulting in an increase in the polarization charge, which in turn increases the effects of EP_{NL}.[93]

This finding is notable because the retention time of a particle (t_R) in an EK system is inversely proportional to the magnitude of its zeta potential.[94] The lower the magnitude of its negative zeta potential, the faster the particle migrates. While the native zeta potential difference between the phage ϕKZ and *E. coli* cells (~25 mV) was sufficient for separation in the linear regime, the binding-induced effects, which reduced the zeta potential magnitude of the *E. coli* cells, widened this gap to ~33 mV, further improving the discrimination capability.

In an iEK channel, two types of separation schemes can occur: streaming separations[31] and streaming–trapping separations.[95] Both types of separations were performed in this study, exploiting the distinct electromigration behavior of the target particles and the effects of nonspecific binding.

Binary separations of a bacteriophage and a microparticle

Binary separation experiments between phage ϕKZ and the synthetic proxy for *P. aeruginosa*, P1 microparticles, were conducted in the iEK channel in Fig. 1 under two distinct electric field strengths. With the computed voltages from the COMSOL model for the injection steps, a series of experiments were con-

ducted to ascertain the optimal duration and voltages for the loading and gating steps (Table 2). Once these parameters were determined, experiments were performed to separate the phage ϕKZ from the P1 microparticles.

First, a separation was performed at a field strength of 194.3 V cm^{-1}. The electropherogram in Fig. 2a shows the phage and P1 microparticle elution peaks with a separation resolution of R_s = 2.41. This baseline separation confirms that the electrophoretic mobility differences enable a charged-based separation by exploiting the differences in zeta potential. Subsequently, the electric field was increased to 430.4 V cm^{-1}, which induced nonlinear EK effects in the P1 microparticles (β = 1.11), while the phages remained in the linear regime. The electropherogram of this separation is shown in Fig. 2b, where a lower separation resolution of R_s = 1.7 was obtained, demonstrating that the separation between ϕKZ and microparticles P1 should be carried out as a charged-based separation in the linear regime. The only advantage offered by performing the separation at a higher electric field is a shorter processing time. Both separations shown in Fig. 2 are charged-based separations, aided by the effects on nonspecific binding, which shifted the zeta potential of the P1 microparticle from −25.5 mV to −20.2 mV (change of 5.3 mV), these effects would not enhance separations in the nonlinear regime.

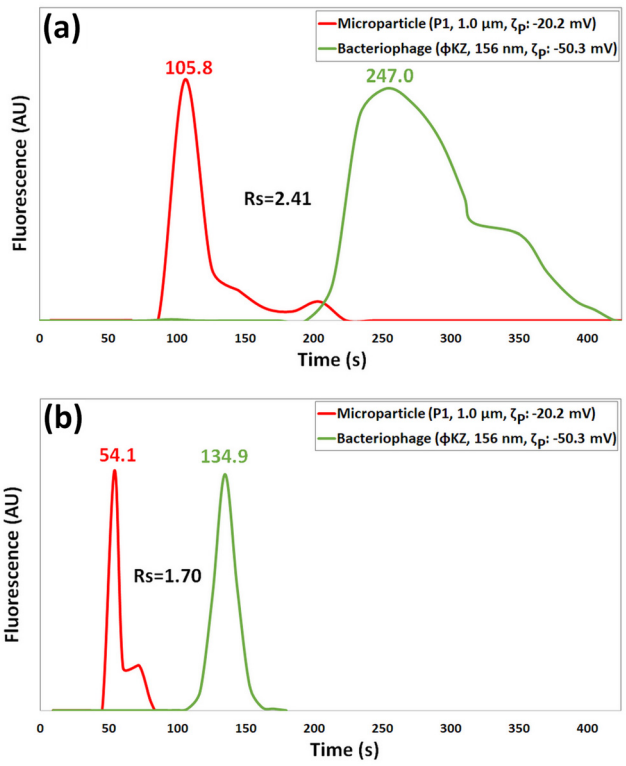

Fig. 2 Electropherograms of the binary separations of phage ϕKZ and microparticles at an electric field strength (computed between the vertical constriction between the posts) of (a) 194.3 V cm^{-1} showing a resolution of R_s = 2.41 and (b) 430.4 V cm^{-1} showing a resolution of R_s = 1.70. All applied voltages are in Table 2.

Binary separations of a bacteriophage and a bacterium

Due to the similarities in particle properties between the two separations, the exact same voltages were used for both types of streaming mode separations, which allowed the evaluation of reproducibility. Separations were initially performed at 194.3 V cm^{-1} and 430.4 V cm^{-1}.

At a lower field of 194.3 V cm^{-1} a separation resolution of R_s = 2.49 was obtained, as shown in the electropherogram in Fig. 3a. The results are similar to those obtained for the ϕKZ-P1 separation (Fig. 2a). In both cases, differences in charge are the discriminating mechanism, although some nonlinear effects may affect the migration of the *E. coli* cells as they migrated under the conditions of β = 0.91. However, the charge difference is the dominating effect in this separation, which was aided by the reduction in the magnitude of the zeta potential of the *E. coli* cells induced by the nonspecific binding.

The electropherogram obtained at 430.4 V cm^{-1}, shown in Fig. 3b, also followed the same trend observed with the ϕKZ-P1 separation (Fig. 2b). A decrease in separation resolution was obtained with an R_s = 1.69, with both analytes exhibiting significantly earlier elution times. The fact that the *E. coli* cells migrated under the effects of nonlinear electrophoresis with β = 2.00 only worsened this charged-based separation. An advantage of using a higher voltage is a faster separation, although at the cost of decreased resolution. Both electropherograms in Fig. 3 are charged-based separations that were aided by the effects of nonspecific binding which shifted the zeta potential of *E. coli* cells from −25.5 mV to −17.6 mV (change of 7.9 mV).

The effects of EP_{NL} can be strategically exploited for the separation between phages and host cells by employing a streaming–trapping approach.[95] In this mode of separation, the host cells —which are influenced by EP_{NL} effects—reach a trapping threshold at the constriction regions between the posts, while the phages continue to flow in a streaming pattern. To illustrate this, an additional experiment was conducted at an electric field of 580.6 V cm^{-1} to induce trapping of *E. coli* cells at β = 2.7. Under these parameters, the ϕKZ phages remained in the linear regime and streamed through the array unimpeded, as demonstrated in Fig. 3c. Under these conditions the elution order is reversed; the phages elute first, followed by a deliberate reduction in the electric field strength to release the trapped *E. coli* cells. Ultimately, this demonstrates that EP_{NL} provides a tunable mechanism for purification, allowing for the selective immobilization of larger, lower-charge analytes while maintaining high-throughput recovery of the target bacteriophages. A detailed analysis of the contribution of each individual EK phenomenon to the overall particle migration in all the separations in this study is included in Fig. S4. From this figure it can be observed that EP_{NL} effects become significant for the P1 microparticles and *E. coli* cells at fields of 430.4 V cm^{-1} and 580.6 V cm^{-1}. Videos of the eluting peaks obtained at 194.3 V cm^{-1} and 430.4 V cm^{-1} were included with the SI as Videos S3 and S4, respectively.

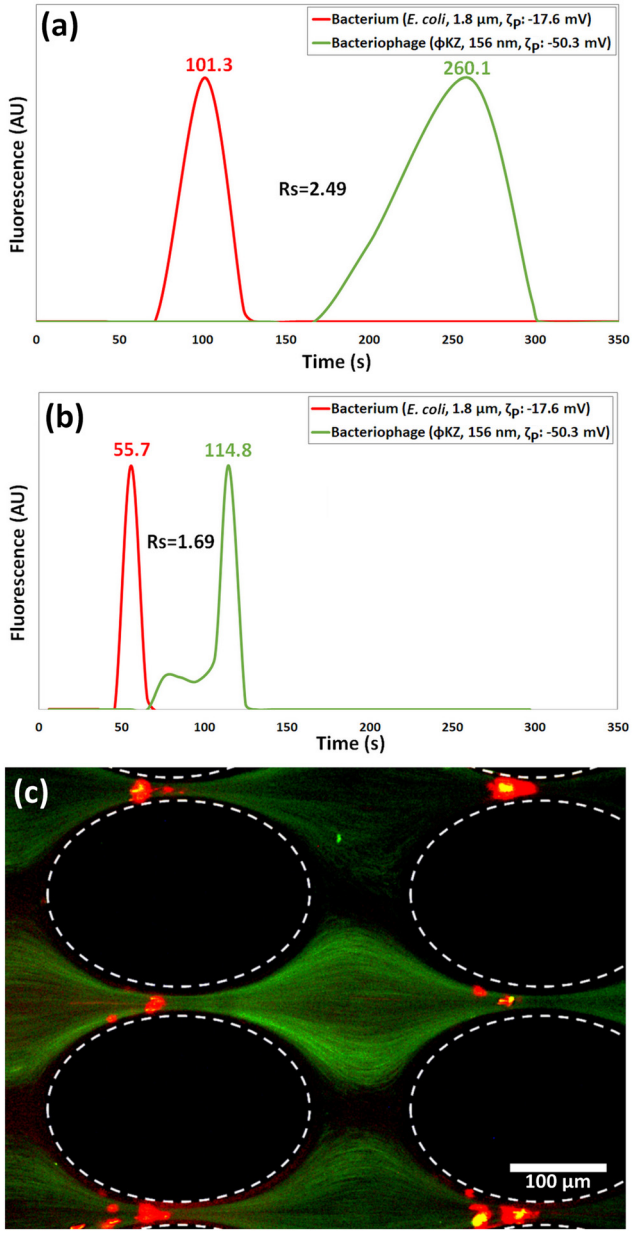

Fig. 3 Electropherograms of the binary separations of phage ϕKZ and *E. coli* cells at an electric field strength (computed between the vertical constriction between the posts) of (a) 194.3 V cm^{-1} showing a resolution of R_s = 2.49 and (b) 430.4 V cm^{-1} showing a resolution of R_s = 1.69; (c) image of trapping–streaming separation of ϕKZ-*E. coli* cells where the red *E. coli* cells are electrokinetically trapped at 580.6 V cm^{-1} while the green ϕKZ streams along. All applied voltages are in Table 2.

Discussion

The ϕKZ elution peaks show distinct shape variations across the four streaming separations. While co-analytes (P1 and *E. coli* cells) remained consistent—exhibiting tailing and Gaussian, respectively—the ϕKZ peak transitioned from tailing at 194.3 V cm^{-1} (Fig. 2a) to Gaussian at 430.4 V cm^{-1} (Fig. 2b). Notably, the ϕKZ peak exhibited fronting behavior in

Table 3 Experimental ($t_{R,e}$) and model-predicted ($t_{R,p}$) retention times with deviations for separating microparticles (P1) and *E. coli* cells from ϕKZ phages, with predictions based on their properties as characterized in the presence of ϕKZ (Table 1). The dimensionless parameters (β, Pe, and Du) were calculated at the post constriction to indicate the operative EK regime for each analyte

Separation ID	Particle ID	Predicted $t_{R,p}$ (s)	Rep 1 $t_{R,e}$ (s)	Rep 2 $t_{R,e}$ (s)	Rep 3 $t_{R,e}$ (s)	Average $\overline{t_{R,e}}$ (s)	% Deviation $t_{R,p}$ *vs.* $\overline{t_{R,e}}$
Separation of ϕKZ and P1 at E = 194.3 V cm^{-1}, avg. R_s = 2.51							
ϕKZ conditions: β = 0.08, Du = 1.54 and Pe = 0.03	P1	127.9	105.8	115.6	105.0	108.8	−18
P1 conditions: β = 0.50, Du = 0.09 and Pe = 0.12	ϕKZ	241.8	253.0	245.9	250.2	249.7	3
Separation of ϕKZ and P1 at E = 430.4 V cm^{-1}, avg. R_s = 1.59							
ϕKZ conditions: β = *0.17*, Du = 1.54 and Pe = 0.08	P1	59.1	54.1	56.7	54.4	55.0	−7
P1 conditions: β = *1.11*, Du = 0.09 and Pe = 0.33	ϕKZ	109.7	134.9	134.0	136.5	135.1	19
Separation of ϕKZ and *E. coli* at E = 194.3 V cm^{-1}, avg. R_s = 2.56							
ϕKZ conditions: β = 0.08, Du = 1.54 and Pe = 0.03	*E. coli*	121.0	101.3	103.8	105.9	104.9	−15
E. coli conditions: β = *0.91*, Du = 0.04 and Pe = 0.08	ϕKZ	241.8	260.1	264.8	267.7	266.3	9
Separation of ϕKZ and *E. coli* at E = 430.4 V cm^{-1}, avg. R_s = 1.74							
ϕKZ conditions: β = 0.17, Du = 1.54 and Pe = 0.08	*E. coli*	58.7	55.7	52.6	57.7	55.3	−6
E. coli conditions: β = 2.00, Du = 0.04 and Pe = 0.77	ϕKZ	109.7	114.8	111.0	117.7	114.5	4

the presence of *E. coli* cells (Fig. 3). These inconsistencies are attributed to field-induced phage agglomeration. As established by Mori *et al.*,[96] the application of a DC electric field polarizes the electric double layer (EDL) of particles in aqueous solution. This polarization creates electric dipoles that generate attractive electrostatic forces, driving particle agglomeration. Since ϕKZ possesses a high zeta potential of −50.3 mV, its dense EDL makes the phages highly polarizable, resulting in significant self-agglomeration and the observed morphological instability in peak shapes. This is evident in Videos S1–S4, where agglomerated phages could be seen exiting the post array at the interrogation window.

Another observation from the experimental results is that ϕKZ bacteriophage virions migrated slower than predicted by COMSOL in both the separations—a discrepancy attributed to limitations in the computational model—whereas the P1 microparticles and *E. coli* cells migrated faster than predicted. As discussed earlier, EK injection bias could be the cause of this deviation. This phenomenon has been observed in other studies when the difference in the zeta potentials of two analytes is sufficient to create an injections bias. This is a preferential migration effect where the particles with a lower zeta potential magnitude surge ahead and elute earlier than anticipated.[31,90,97] Given that the EK injection voltages and durations were the same for both sets of streaming of separations, the particles with lower zeta potential magnitudes (P1 microparticles and *E. coli* cells) exhibited consistent tendencies by eluting earlier than expected. This observation reinforces the EK injection bias theory, demonstrating that analytes with reduced electrophoretic mobility are preferentially surged forward by the electroosmotic flow during the injection phase.

It is important to note that the model has limitations, as detailed in the mathematical model section. Specifically, the simulations do not account for particle–particle interactions, Joule heating or EK injection bias effects. Despite these omissions, the primary utility of the model is to guide experimentation, by identifying appropriate operational voltages for separations. Considering that the separations occurred using the exact voltages that the model predicted and that the deviation between predicted and experimental times is consistently below 20% (Table 3), the model is a valuable tool for streamlining experiments and eliminating the need for trial-and-error methodologies.

Conclusions

This study demonstrated the successful charged-based separation of bacteriophage ϕKZ from polystyrene microparticles and *E. coli* cells. Given the significantly higher zeta potential magnitude of the phages, both the polystyrene microparticles and *E. coli* cells eluted first in the streaming experiments. The effects of the nonspecific binding affinity between the phage tails and the surface of the co-analytes were quantified.[67,68] This characterization revealed that the formation of phage complexes results in a reduction in the magnitude of the zeta potential (~8 mV or 30% for *E. coli* cells). This surface modification is a quantifiable factor influencing their migration behavior, which aided the charged-based separations reported in this work.

For each binary system (ϕKZ-P1 and ϕKZ-*E. coli* cells), two sets of streaming binary separations were carried out at the field strengths of 194.3 V cm^{-1} and 430.4 V cm^{-1}. The separations at the lower field strength (194.3 V cm^{-1}) yielded better resolution, as charged-based separations are the most efficient when all analytes migrate within the linear electrophoretic regime. This is further supported by the lower separation resolution values obtained at the higher field strength (430.4 V cm^{-1}) for both systems. While employing a higher field resulted in faster separation times, it compromised resolution; in this case, the emergence of nonlinear electrophoresis effects proved detrimental to the charge-based separation efficiency.

An additional separation under the streaming–trapping regime was carried out to demonstrate the strategic application of nonlinear electrophoresis effects. To induce trapping of *E. coli* cells, a field of 580.6 V cm^{-1} was used, triggering strong nonlinear electrophoresis effects that trapped the cells within the post array, while the ϕKZ phages flowed unimpeded in a streaming fashion. In this regime, the elution order is reversed: the phages elute first, while the cells remain trapped. Cell recovery is subsequently achieved by reducing the field to release the cells from the trapping regions. These results illustrate that nonlinear electrophoresis is a tunable mechanism for phage purification, as it allows for the selective immobilization of host cells based on their specific electrokinetic thresholds.

In future research, the electrokinetic effects of nonspecific binding between bacteriophages and synthetic or biological particles will be investigated to understand the broader implications of this phenomenon. For instance, electrokinetics presents a potential strategy to investigate the mechanisms behind the changes in bacterial motility in the environment, as comparable cases were observed by Ping *et al.*[98] and Yu *et al.*[99] Another consideration is the potential loss of ϕKZ titer due to its nonspecific binding affinities for synthetic and bacterial surfaces. Further investigations are required to quantify the degree of sample loss, which must be weighed against strategies to passivate the binding sites. Efforts are also underway to develop methods for the removal of cellular debris from phage samples. As discussed earlier, highly purified bacteriophage preparations are required for phage therapy, as the presence of host cell debris and other endotoxins could induce adverse effects in patients.[15] Developing an adaptable and cost-effective electrokinetic-based solution that overcomes the limitations of current methodologies is paramount to achieving a wider prevalence of phage therapy for nosocomial infections.

Author contributions

Viswateja Kasarabada: software, validation, formal analysis, investigation, data curation, writing – original draft, writing –

review & editing, and visualization. Zakia Azad: formal analysis, investigation, writing – original draft, and writing – review & editing. Julie A. Thomas: conceptualization, methodology, writing – original draft, writing – review & editing, visualization, supervision, project administration, and funding acquisition. Blanca H. Lapizco-Encinas: conceptualization, methodology, writing – original draft, writing – review & editing, visualization, supervision, project administration, and funding acquisition.

Conflicts of interest

There are no conflicts to declare.

Data availability

The data supporting this article have been included as part of the supplementary information (SI). Supplementary information is available. In addition to the supplementary information file, we provided four videos as supplementary videos for the experiments. See DOI: https://doi.org/10.1039/d5an01220a.

Acknowledgements

This material is based upon work supported by the National Science Foundation under Award No. 2133207. The authors acknowledge Research Computing at the Rochester Institute of Technology for providing computational resources and support that have contributed to the research results reported in this publication.

References

1 M. P. William and A. Rutala, Ph.D., *Healthc. Infect. Control Pract. Advis. Comm.*, 2017, 1–158.
2 S. A. Alali, E. Shrestha, A. R. Kansakar, A. Parekh, S. Dadkhah and W. F. Peacock, Community hospital stethoscope cleaning practices and contamination rates, *Am. J. Infect. Control*, 2020, **48**, 1365–1369.
3 A. Sulakvelidze, Z. Alavidze and J. Morris, Bacteriophage therapy, *Antimicrob. Agents Chemother.*, 2001, **45**, 649–659.
4 M. R. J. Clokie, A. D. Millard, A. V. Letarov and S. Heaphy, Phages in nature, *Bacteriophage*, 2011, **1**, 31.
5 E. C. Keen, A century of phage research: Bacteriophages and the shaping of modern biology, *BioEssays*, 2014, **37**, 6–9.
6 N. Chanishvili, *Phage Therapy-History from Twort and d'Herelle Through Soviet Experience to Current Approaches*, Elsevier Inc., 1st edn., 2012, vol. 83.
7 C. Suttle, Crystal ball. The viriosphere: the greatest biological diversity on Earth and driver of global processes., *Environ. Microbiol.*, 2005, **7**, 481–482.
8 R. W. Hendrix, in *Current Topics in Microbiology and Immunology*, ed. J. L. Van Etten, Springer Berlin Heidelberg, Berlin, Heidelberg, 2009, vol. 328, pp. 229–240.
9 R. Monson, I. Foulds, J. Foweraker, M. Welch and G. P. C. Salmond, The Pseudomonas aeruginosa generalized transducing phage ϕPA3 is a new member of the ϕKZ-like group of 'jumbo' phages, and infects model laboratory strains and clinical isolates from cystic fibrosis patients, *Microbiology*, 2011, **157**, 859–867.
10 D. Reynolds and M. Kollef, The Epidemiology and Pathogenesis and Treatment of Pseudomonas aeruginosa Infections: An Update, *Drugs*, 2021, **81**, 2117–2131.
11 T. K. Lu and M. S. Koeris, The next generation of bacteriophage therapy, *Curr. Opin. Microbiol.*, 2011, **14**, 524–531.
12 V. V. Mesyanzhinov, J. Robben, B. Grymonprez, V. A. Kostyuchenko, M. V. Bourkaltseva, N. N. Sykilinda, V. N. Krylov and G. Volckaert, The genome of bacteriophage ϕKZ of Pseudomonas aeruginosa, *J. Mol. Biol.*, 2002, **317**, 1–19.
13 L. Endersen, J. O'Mahony, C. Hill, R. P. Ross, O. McAuliffe and A. Coffey, Phage Therapy in the Food Industry, *Annu. Rev. Food Sci. Technol.*, 2014, **5**, 327–349.
14 M. P. Nikolich and A. A. Filippov, Bacteriophage therapy: Developments and directions, *Antibiotics*, 2020, **9**, 135.
15 B. Zalewska-pi, *Phage Therapy—Challenges, Opportunities and Future Prospects*, 2023, pp. 1–20.
16 V. Clavijo, M. A. Torres-Acosta, M. J. Vives-Flórez and M. Rito-Palomares, Aqueous two-phase systems for the recovery and purification of phage therapy products: Recovery of salmonella bacteriophage ϕSan23 as a case study, *Sep. Purif. Technol.*, 2019, **211**, 322–329.
17 A. Carroll-Portillo, C. N. Coffman, M. G. Varga, J. Alcock, S. B. Singh and H. C. Lin, Standard bacteriophage purification procedures cause loss in numbers and activity, *Viruses*, 2021, **13**, 328.
18 N. Bonilla, M. I. Rojas, G. N. F. Cruz, S.-H. Hung, F. Rohwer and J. J. Barr, Phage on tap-a quick and efficient protocol for the preparation of bacteriophage laboratory stocks, *PeerJ*, 2016, **4**, e2261.
19 T. Nasukawa, J. Uchiyama, S. Taharaguchi, S. Ota, T. Ujihara, S. Matsuzaki, H. Murakami, K. Mizukami and M. Sakaguchi, Virus purification by CsCl density gradient using general centrifugation, *Arch. Virol.*, 2017, **162**, 3523–3528.
20 V. Štilec, M. Marušić, N. Janež, U. Bezeljak, L. Rebula, M. Leskovec, R. Trebše, S. Horvat and M. Peterka, Preparation and pharmacokinetic evaluation of Staphylococcus phage COP-80B for treatment of periprosthetic joint infections in a mouse model, *Virus Res.*, 2025, **357**, 199592.
21 T. Luong, A. C. Salabarria, R. A. Edwards and D. R. Roach, Standardized bacteriophage purification for personalized phage therapy, *Nat. Protoc.*, 2020, **15**, 2867–2890.
22 G. Bourdin, B. Schmitt, L. M. Guy, J. E. Germond, S. Zuber, L. Michot, G. Reuteler and H. Brüssow, Amplification and purification of T4-Like Escherichia coli phages for phage

therapy: From laboratory to pilot scale, *Appl. Environ. Microbiol.*, 2014, **80**, 1469–1476.
23 V. Hietala, J. Horsma-Heikkinen, A. Carron, M. Skurnik and S. Kiljunen, The Removal of Endo- and Enterotoxins From Bacteriophage Preparations, *Front. Microbiol.*, 2019, **10**, 1674.
24 J. P. P. Saavedra, A. R. Silva-Santos, S. O. D. Duarte and A. M. Azevedo, Scalable purification of bacteriophages preparations, *J. Chromatogr. A*, 2025, **1749**, 1–10.
25 R. Roshankhah, K. Jackson, T. T. N. Nguyen, R. Pelton, Z. Hosseinidoust and R. Ghosh, Purification of phage for therapeutic applications using high throughput anion exchange membrane chromatography, *J. Chromatogr. B*, 2023, **1229**, 123867.
26 S. S. Binte Mohamed Yakob Adil, J. Tucci, H. Irving, C. Cianciarulo and M. Kabwe, Evaluation of effectiveness of bacteriophage purification methods, *Virol. J.*, 2024, **21**, 318.
27 A. Carroll-Portillo, C. N. Coffman, M. G. Varga, J. Alcock, S. B. Singh and H. C. Lin, Standard bacteriophage purification procedures cause loss in numbers and activity, *Viruses*, 2021, **13**, 328.
28 M. D. C. Pons Royo and A. Jungbauer, Polyethylene glycol precipitation: fundamentals and recent advances, *Prep. Biochem. Biotechnol.*, 2025, **55**, 935–954.
29 J. H. Moore, C. Honrado, V. Stagnaro, G. Kolling, C. A. Warren and N. S. Swami, Rapid in Vitro Assessment of Clostridioides difficile Inhibition by Probiotics Using Dielectrophoresis to Quantify Cell Structure Alterations, *ACS Infect. Dis.*, 2020, **6**, 1000–1007.
30 L. Huang, F. Liang, Y. Feng, P. Zhao and W. Wang, On-chip integrated optical stretching and electrorotation enabling single-cell biophysical analysis, *Microsyst. Nanoeng.*, 2020, **6**, 1–14.
31 A. Vaghef-Koodehi, C. Dillis and B. H. Lapizco-Encinas, High-Resolution Charge-Based Electrokinetic Separation of Almost Identical Microparticles, *Anal. Chem.*, 2022, **94**, 6451–6456.
32 B. H. Lapizco-Encinas, Nonlinear Electrokinetic Methods of Particles and Cells, *Annu. Rev. Anal. Chem.*, 2024, **17**, 243–264.
33 B. H. Lapizco-Encinas, Recent developments in the use of electrokinetic methods for rapid cell viability assessments and separations, *J. Chromatogr. Open*, 2024, **6**, 100185.
34 S. Yan, Z. Rajestari, T. C. Morse, H. Li and L. Kulinsky, Electrokinetic Manipulation of Biological Cells towards Biotechnology Applications, *Micromachines*, 2024, **15**, 341.
35 A. Tiselius, A new apparatus for electrophoretic analysis of colloidal mixtures, *Trans. Faraday Soc.*, 1937, **33**, 524–531.
36 A. Vaghef-Koodehi and B. H. Lapizco-Encinas, Microscale electrokinetic-based analysis of intact cells and viruses, *Electrophoresis*, 2022, **43**, 263–287.
37 A. Vaghef-Koodehi and B. H. Lapizco-Encinas, Switching Separation Migration Order by Switching Electrokinetic Regime in Electrokinetic Microsystems, *Biosensors*, 2024, **14**, 119.
38 A. Vaghef-Koodehi and B. H. Lapizco-Encinas, Tuning the Migration Order in Electrokinetic Separations of Saccharomyces cerevisiae Cells, *Anal. Chem.*, 2025, **97**, 10433–10441.
39 A. S. Khair, Nonlinear electrophoresis of colloidal particles, *Curr. Opin. Colloid Interface Sci.*, 2022, **59**, 101587.
40 C. A. Mendiola-Escobedo and B. H. Lapizco-Encinas, Fifty Years of Nonlinear Electrophoresis, *Electrophoresis*, 2025, **46**, 1548–1564.
41 S. S. Dukhin, Non-equilibrium electric surface phenomena, *Adv. Colloid Interface Sci.*, 1993, **44**, 1–134.
42 S. S. Dukhin, Electrophoresis at large peclet numbers, *Adv. Colloid Interface Sci.*, 1991, **36**, 219–248.
43 N. A. Mishchuk and S. S. Dukhin, Electrophoresis of solid particles at large Peclet numbers, *Electrophoresis*, 2002, **23**, 2012–2022.
44 S. S. Dukhin, Electrokinetic phenomena of the second kind and their applications, *Adv. Colloid Interface Sci.*, 1991, **35**, 173–196.
45 M. Rouhi Youssefi and F. J. Diez, Ultrafast electrokinetics, *Electrophoresis*, 2016, **37**, 692–698.
46 B. Cardenas-Benitez, B. Jind, R. C. Gallo-Villanueva, S. O. Martinez-Chapa, B. H. Lapizco-Encinas and V. H. Perez-Gonzalez, Direct Current Electrokinetic Particle Trapping in Insulator-Based Microfluidics: Theory and Experiments, *Anal. Chem.*, 2020, **92**, 12871–12879.
47 S. Tottori, K. Misiunas, U. F. Keyser and D. J. Bonthuis, Nonlinear Electrophoresis of Highly Charged Nonpolarizable Particles, *Phys. Rev. Lett.*, 2019, **123**, 14502.
48 J. B. Bancroft, Purification and properties of bean pod mottle virus and associated centrifugal and electrophoretic components., *Virology*, 1962, **16**, 419–427.
49 L. Kremser, D. Blaas and E. Kenndler, Virus analysis using electromigration techniques, *Electrophoresis*, 2009, **30**, 133–140.
50 L. Kremser, D. Blaas and E. Kenndler, Capillary electrophoresis of biological particles: Viruses, bacteria, and eukaryotic cells, *Electrophoresis*, 2004, **25**, 2282–2291.
51 P. Serwer and S. J. Hayes, Agarose gel electrophoresis of bacteriophages and related particles, *J. Chromatogr. B: Biomed. Sci. Appl.*, 1982, **3**, 76–80.
52 R. E. Fernandez, A. Rohani, V. Farmehini and N. S. Swami, Review: Microbial analysis in dielectrophoretic microfluidic systems, *Anal. Chim. Acta*, 2017, **966**, 11–33.
53 M. P. Hughes, H. Morgan, F. J. Rixon, J. P. H. Burt and R. Pethig, Manipulation of herpes simplex virus type 1 by dielectrophoresis, *Biochim. Biophys. Acta, Gen. Subj.*, 1998, **1425**, 119–126.
54 M. P. Hughes, H. Morgan and F. J. Rixon, Measuring the dielectric properties of herpes simplex virus type 1 virions with dielectrophoresis, *Biochim. Biophys. Acta, Gen. Subj.*, 2002, **1571**, 1–8.
55 M. P. Hughes, H. Morgan and F. J. Rixon, in 20th Annual International Conference of the IEEE Engineering in Medicine and Biology Society, 1998, vol. 20(6), pp. 2816–2819.

56 H. Morgan, M. P. Hughes and N. G. Green, Separation of submicron bioparticles by dielectrophoresis, *Biophys. J.*, 1999, **77**, 516–525.
57 C. V. Crowther and M. A. Hayes, Refinement of insulator-based dielectrophoresis, *Analyst*, 2017, **142**, 1608–1618.
58 A. K. M. F. K. Rasel, E. P. Ristich, M. A. Hayes and S. L. Seyler, Streaming-Particle Method for Dielectrophoretic Characterization, *Electrophoresis*, 2025, **46**, 1341–1357.
59 J. Ding, R. M. Lawrence, P. V. Jones, B. G. Hogue and M. A. Hayes, Concentration of Sindbis virus with optimized gradient insulator-based dielectrophoresis, *Analyst*, 2016, **141**, 1997–2008.
60 A. Coll De Peña, N. H. Mohd Redzuan, M. Abajorga, N. Hill, J. A. Thomas and B. H. Lapizco-Encinas, Analysis of bacteriophages with insulator-based dielectrophoresis, *Micromachines*, 2019, **10**, 450.
61 V. Kasarabada, N. N. Nasir Ahamed, A. Vaghef-Koodehi, G. Martinez-Martinez and B. H. Lapizco-Encinas, Separating the Living from the Dead: An Electrophoretic Approach, *Anal. Chem.*, 2024, **96**, 15711–15719.
62 A. Lomeli-Martin, Z. Azad, J. A. Thomas and B. H. Lapizco-Encinas, Assessment of the Nonlinear Electrophoretic Migration of Nanoparticles and Bacteriophages, *Micromachines*, 2024, **15**, 369.
63 I. J. Clifton and D. G. Peckham, Defining routes of airborne transmission of Pseudomonas aeruginosa in people with cystic fibrosis, *Expert Rev. Respir. Med.*, 2010, **4**, 519–529.
64 G. M. Bruinsma, M. Rustema-Abbing, H. C. van der Mei, C. Lakkis and H. J. Busscher, Resistance to a polyquaternium-1 lens care solution and isoelectric points of Pseudomonas aeruginosa strains, *J. Antimicrob. Chemother.*, 2006, **57**, 764–766.
65 Y. Tashiro, S. Ichikawa, M. Shimizu, M. Toyofuku, N. Takaya, T. Nakajima-Kambe, H. Uchiyama and N. Nomura, Variation of physiochemical properties and cell association activity of membrane vesicles with growth phase in Pseudomonas aeruginosa, *Appl. Environ. Microbiol.*, 2010, **76**, 3732–3739.
66 S. P. Diggle and M. Whiteley, Microbe profile: Pseudomonas aeruginosa: Opportunistic pathogen and lab rat, *Microbiology*, 2020, **166**, 30–33.
67 H. L. Marton, P. Kilbride, A. Ahmad, A. P. Sagona and M. I. Gibson, Anionic Synthetic Polymers Prevent Bacteriophage Infection, *J. Am. Chem. Soc.*, 2023, **145**, 8794–8799.
68 Y. Briers, G. Volckaert, A. Cornelissen, S. Lagaert, C. W. Michiels, K. Hertveldt and R. Lavigne, Muralytic activity and modular structure of the endolysins of Pseudomonas aeruginosa bacteriophages ϕKZ and EL, *Mol. Microbiol.*, 2007, **65**, 1334–1344.
69 R. Cademartiri, H. Anany, I. Gross, R. Bhayani, M. Griffiths and M. A. Brook, Immobilization of bacteriophages on modified silica particles, *Biomaterials*, 2010, **31**, 1904–1910.
70 O. Zemb, M. Manefield, F. Thomas and S. Jacquet, Phage adsorption to bacteria in the light of the electrostatics: A case study using *E. coli*, T2 and flow cytometry, *J. Virol. Methods*, 2013, **189**, 283–289.
71 H. Anany, W. Chen, R. Pelton and M. W. Griffiths, Biocontrol of Listeria monocytogenes and Escherichia coli O157:H7 in meat by using phages immobilized on modified cellulose membranes, *Appl. Environ. Microbiol.*, 2011, **77**, 6379–6387.
72 V. Krylov, M. Bourkaltseva, E. Pleteneva, O. Shaburova, S. Krylov, A. Karaulov, S. Zhavoronok, O. Svitich and V. Zverev, Phage phiKZ-The First of Giants, *Viruses*, 2021, **13**, 149.
73 A. Fokine, A. J. Battisti, V. D. Bowman, A. V. Efimov, L. P. Kurochkina, P. R. Chipman, V. V. Mesyanzhinov and M. G. Rossmann, Cryo-EM Study of the Pseudomonas Bacteriophage ϕKZ, *Structure*, 2007, **15**, 1099–1104.
74 A. Fokine, V. A. Kostyuchenko, A. V. Efimov, L. P. Kurochkina, N. N. Sykilinda, J. Robben, G. Volckaert, A. Hoenger, P. R. Chipman, A. J. Battisti, M. G. Rossmann and V. V. Mesyanzhinov, A Three-dimensional Cryo-electron Microscopy Structure of the Bacteriophage ϕKZ Head, *J. Mol. Biol.*, 2005, **352**, 117–124.
75 B. Ali, M. I. Desmond, S. A. Mallory, A. D. Benítez, L. J. Buckley, S. T. Weintraub, M. V. Osier, L. W. Black and J. A. Thomas, To be or not to be T4: Evidence of a complex evolutionary pathway of head structure and assembly in giant Salmonella virus SPN3US, *Front. Microbiol.*, 2017, **8**, 2251.
76 K. Hertveldt, R. Lavigne, E. Pleteneva, N. Sernova, L. Kurochkina, R. Korchevskii, J. Robben, V. Mesyanzhinov, V. N. Krylov and G. Volckaert, Genome comparison of Pseudomonas aeruginosa large phages, *J. Mol. Biol.*, 2005, **354**, 536–545.
77 P. Dutta and A. Beskok, Analytical solution of combined electroosmotic/pressure driven flows in two-dimensional straight channels: Finite Debye layer effects, *Anal. Chem.*, 2001, **73**, 1979–1986.
78 H. Ohshima, A simple expression for henry's function for the retardation effect in electrophoresis of spherical colloidal particles, *J. Colloid Interface Sci.*, 1994, **168**, 269–271.
79 O. Schnitzer and E. Yariv, Nonlinear electrophoresis at arbitrary field strengths: Small-Dukhin-number analysis, *Phys. Fluids*, 2014, **26**, 122002.
80 O. Schnitzer, R. Zeyde, I. Yavneh and E. Yariv, Weakly nonlinear electrophoresis of a highly charged colloidal particle, *Phys. Fluids*, 2013, **25**, 052004.
81 R. Cobos and A. S. Khair, Nonlinear electrophoretic velocity of a spherical colloidal particle, *J. Fluid Mech.*, 2023, **968**, A14.
82 J. Bentor, H. Dort, R. A. Chitrao, Y. Zhang and X. Xuan, Nonlinear electrophoresis of dielectric particles in Newtonian fluids, *Electrophoresis*, 2023, **44**, 938–946.
83 J. Bentor and X. Xuan, Nonlinear electrophoresis of non-spherical particles in a rectangular microchannel, *Electrophoresis*, 2024, **45**, 712–719.
84 M. A. Saucedo-Espinosa and B. H. Lapizco-Encinas, Refinement of current monitoring methodology for electro-

osmotic flow assessment under low ionic strength conditions, *Biomicrofluidics*, 2016, **10**, 033104.
85 O. D. Ernst, A. Vaghef-Koodehi, C. Dillis, A. Lomeli-Martin and B. H. Lapizco-Encinas, Dependence of Nonlinear Electrophoresis on Particle Size and Electrical Charge, *Anal. Chem.*, 2023, **95**, 6595–6602.
86 S. Antunez-Vela, V. H. Perez-Gonzalez, A. Coll De Peña, C. J. Lentz and B. H. Lapizco-Encinas, Simultaneous Determination of Linear and Nonlinear Electrophoretic Mobilities of Cells and Microparticles, *Anal. Chem.*, 2020, **92**, 14885–14891.
87 A. Miller, N. Hill, K. Hakim and B. H. Lapizco-Encinas, Fine–tuning electrokinetic injections considering nonlinear electrokinetic effects in insulator–based devices, *Micromachines*, 2021, **12**, 628.
88 M. A. Saucedo-Espinosa, A. Lalonde, A. Gencoglu, M. F. Romero-Creel, J. R. Dolas and B. H. Lapizco-Encinas, Dielectrophoretic manipulation of particle mixtures employing asymmetric insulating posts, *Electrophoresis*, 2016, **37**, 282–290.
89 D. Brown, in Poster presented at the AAPT 2005 Summer Meeting, August 6–11, 2005, https://www.compadre.org/OSP/items/detail.cfm?ID=9685, Salt Lake City, Utah, United States, 2005, pp. 1–11.
90 A. Vaghef-Koodehi, P. Cyr and B. H. Lapizco-Encinas, Improving device design in insulator-based electrokinetic tertiary separations, *J. Chromatogr. A*, 2024, **1722**, 464853.
91 M. C. Breadmore, *Bioanalysis*, 2009, **1**, 889–894.
92 L.-M. Fu and C.-H. Tsai, *Encyclopedia of Microfluidics and Nanofluidics*, Springer US, 2014, pp. 1–10.
93 N. A. Mishchuk and N. O. Barinova, Theoretical and experimental study of nonlinear electrophoresis, *Colloid J.*, 2011, **73**, 88–96.
94 A. Vaghef-Koodehi, V. H. Perez-Gonzalez and B. H. Lapizco-Encinas, Predicting the retention time of microparticles in electrokinetic migration, *Analyst*, 2025, **150**, 3626–3635.
95 H. Moncada-Hernández and B. H. Lapizco-Encinas, Simultaneous concentration and separation of microorganisms: Insulator-based dielectrophoretic approach, *Anal. Bioanal. Chem.*, 2010, **396**, 1805–1816.
96 T. Mori, H. Nagashima, Y. Ito, Y. Era and J. I. Tsubaki, Agglomeration of fine particles in water upon application of DC electric field, *Miner. Eng.*, 2019, **133**, 119–126.
97 A. Vaghef-Koodehi, O. D. Ernst and B. H. Lapizco-Encinas, Separation of Cells and Microparticles in Insulator-Based Electrokinetic Systems, *Anal. Chem.*, 2023, **95**, 1409–1418.
98 D. Ping, T. Wang, D. T. Fraebel, S. Maslov, K. Sneppen and S. Kuehn, Hitchhiking, collapse, and contingency in phage infections of migrating bacterial populations, *ISME J.*, 2020, **14**, 2007–2018.
99 Z. Yu, C. Schwarz, L. Zhu, L. Chen, Y. Shen and P. Yu, Hitchhiking behavior in bacteriophages facilitates phage infection and enhances carrier bacteria colonization, *Environ. Sci. Technol.*, 2021, **55**, 2462–2472.